Crystal structures of fibronectin-binding sites from *Staphylococcus aureus* FnBPA in complex with fibronectin domains

Richard J. Bingham*, Enrique Rudiño-Piñera[†‡], Nicola A. G. Meenan*, Ulrich Schwarz-Linek[§], Johan P. Turkenburg[¶], Magnus Höök[‖], Elspeth F. Garman[‡], and Jennifer R. Potts*[¶**]**

*Department of Biology, University of York, PO Box 373, York YO10 5YW, United Kingdom; [†]Departamento de Medicina Molecular y Bioprocesos, Instituto de Biotecnología, Universidad Nacional Autónoma de México, P. O. Box 510-3 Cuernavaca, MOR 62271, Mexico; [‡]Department of Biochemistry, University of Oxford, South Parks Road, Oxford OX1 3QU, United Kingdom; [§]Centre for Biomolecular Sciences, University of St. Andrews, North Haugh, St. Andrews, Fife KY16 9ST, United Kingdom; [¶]Structural Biology Laboratory, Department of Chemistry, University of York, York YO10 5DD, United Kingdom; and [‖]Center for Extracellular Matrix Biology, Institute of Biosciences and Technology, Texas A&M University System Health Science Center, Houston, TX 77030-3303

Edited by Richard O. Hynes, Massachusetts Institute of Technology, Cambridge, MA, and approved June 11, 2008 (received for review April 11, 2008)

Staphylococcus aureus **can adhere to and invade endothelial cells by binding to the human protein fibronectin (Fn). FnBPA and FnBPB, cell wall-attached proteins from *S. aureus*, have multiple, intrinsically disordered, high-affinity binding repeats (FnBRs) for Fn. Here, 30 years after the first report of *S. aureus*/Fn interactions, we present four crystal structures that together comprise the structures of two complete FnBRs, each in complex with four of the N-terminal modules of Fn. Each ≈40-residue FnBR forms antiparallel strands along the triple-stranded β-sheets of four sequential F1 modules ($^{2-5}$F1) with each FnBR/$^{2-5}$F1 interface burying a total surface area of ≈4,300 Å^2. The structures reveal the roles of residues conserved between *S. aureus* and *Streptococcus pyogenes* FnBRs and show that there are few linker residues between FnBRs. The ability to form large intermolecular interfaces with relatively few residues has been proposed to be a feature of disordered proteins, and *S. aureus*/Fn interactions provide an unusual illustration of this efficiency.**

intrinsic disorder | tandem β-zipper | host–pathogen interaction

Staphylococcus aureus is a dangerous human pathogen that causes a wide range of debilitating and life-threatening infections (1). Incidence of *S. aureus* resistance to antibiotics (2) makes the understanding of its mechanisms of pathogenesis imperative. *S. aureus*/Fn interactions were first reported 30 years ago, and an *S. aureus* Fn-binding protein was isolated and characterized ≈20 years ago (3). Our recent work has dissected the 363-residue C-terminal region of FnBPA into 11 FnBRs (4) (FnBPA_1–11; Fig. 1 *A* and *B*), six of which bind the NTD (N-terminal domain) of Fn (comprising modules $^{1-5}$F1) with dissociation constants in the nanomolar range (5). The C-terminal region of FnBPB, a second *S. aureus* Fn-binding protein, is very similar to FnBPA but lacks one of the shorter FnBRs (5). In FnBPA, which also binds fibrinogen, the fibrinogen- and Fn-binding regions (Fig. 1*A*) appear to cooperate in disease progression, with the FnBR region being particularly associated with persistence of infection (6). FnBPA/Fn interactions both mediate *S. aureus* invasion of (7) and activate endothelial cells, evoking both the proinflammatory and procoagulant responses typical of infective endocarditis (8). FnBPAs ability to mediate platelet activation, a key step in thrombus formation, is also likely to play a role in cardiovascular disease (9) and FnBPA has been implicated in cardiac device infections through its ability to mediate *S. aureus* attachment to implanted prosthetic materials (10). We previously predicted that in FnBPA each FnBR binds a string of three or four F1 modules in the NTD of Fn through a longer version of the tandem β-zipper mechanism that we discovered in *Streptococcus dysgalactiae* interactions with ^{1}F1^{2}F1 (4).

Results and Discussion

Crystal Structure of FnBPA-1/$^{2-5}$F1. Fig. 1*C* shows two F1 module pair/peptide structures that together comprise the structure of the most N-terminal *S. aureus* FnBR (FnBPA-1) in complex with $^{2-5}$F1 of Fn. The ^{2}F1^{3}F1/STATT1 and ^{4}F1^{5}F1/STAFF1 complexes were solved to resolutions of 2 and 1.8 Å, respectively. The *S. aureus* peptide binds Fn through four short bacterial motifs that add an antiparallel strand along strand E of the triple-stranded β-sheet (strands CDE; Fig. 1*C*) of the four sequential F1 modules: a tandem β-zipper. A large surface area (11) (≈4,400 Å^2) is buried in the complex and there is a high-interface area per bacterial peptide residue (12). The F1 module structures are very similar for the free and peptide-bound forms. For example, the RMSD between ^{2}F1^{3}F1/STATT1 and ^{2}F1^{3}F1 (PDB ID code 2CG7) for the 43 Cα atoms of ^{2}F1 is 0.67 Å.

There are several examples of β-strand addition in protein–protein interactions (13). However, β-sheet augmentation in a tandem arrangement, as seen in the bacterial peptide/Fn interactions studied here, is very unusual. Only one other example, a LIM domain/peptide complex (14), has been reported.

Crystal Structure of FnBPA-5/$^{2-5}$F1. Fig. 1*D* shows the crystal structure of the complexes between ^{2}F1^{3}F1/STATT5 and ^{4}F1^{5}F1/STAFF5 that together comprise a second complete binding site between Fn and FnBPA. The ^{2}F1^{3}F1/STATT5 and ^{4}F1^{5}F1/STAFF5 structures were solved to resolutions of 1.7 and 2 Å, respectively. These structures confirm that other Fn-binding sites in FnBPA also bind through this unusual tandem β-zipper mechanism. The total surface area buried is ≈4,200 Å^2.

Although it seems clear, based on the relative K_Ds of FnBR/$^{2-5}$F1 and peptide/module interactions (4, 15), that the full FnBPA-1/$^{2-5}$F1 and FnBPA-5/$^{2-5}$F1 interactions can largely be dissected in this way, we have only approximated the relative domain orientations of ^{3}F1 and ^{4}F1 in the intact complex. In addition, the FnBRs in the intact bacterial protein are likely to have less flexible N and C termini, which might influence their

Author contributions: R.J.B., U.S.-L., M.H., E.F.G., and J.R.P. designed research; R.J.B., E.R.-P., and N.A.G.M. performed research; R.J.B. and J.P.T. analyzed data; and R.J.B, E.F.G., and J.R.P. wrote the paper.

The authors declare no conflict of interest.

This article is a PNAS Direct Submission.

Freely available online through the PNAS open access option.

Data deposition: The atomic coordinates have been deposited in the Protein Data Bank , www.pdb.org (PDB ID codes: 2RKZ, 3CAL, 2RKY, and 2RLO).

**To whom correspondence may be addressed. E-mail: elspeth.garman@biop.ox.ac.uk or jp516@york.ac.uk.

This article contains supporting information online at www.pnas.org/cgi/content/full/0803556105/DCSupplemental.

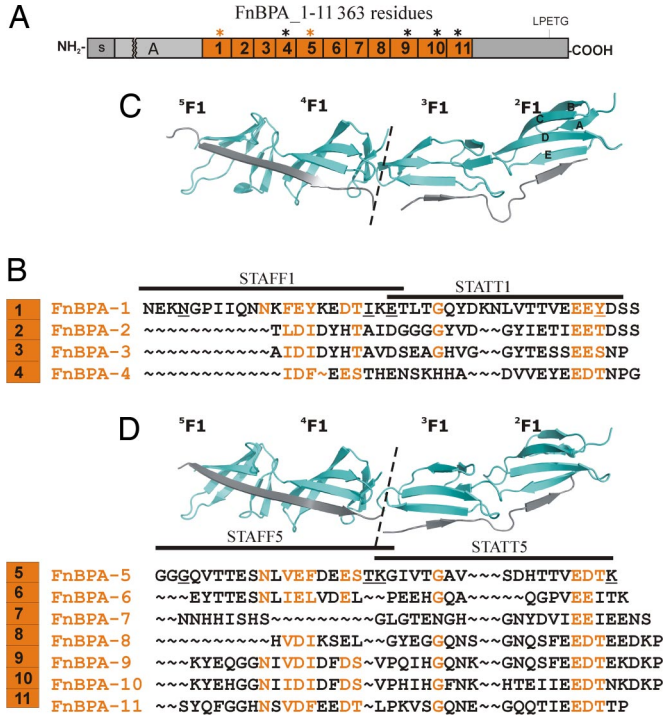

Fig. 1. FnBR peptides from *S. aureus* FnBPA in complex with NTD F1 module pairs from Fn. (*A*) FnBPA contains 11 FnBRs (4), 6 of which bind the NTD of Fn with high affinity (5) (indicated with asterisks, an orange asterisk indicates an FnBR for which structural data are presented). The fibrinogen-binding A domain and the C-terminal bacterial cell-wall attachment site (LPETG) are indicated. (*B*) Sequence alignment of FnBRs from *A* (residues 508–874 of Swiss-Prot entry P14738) highlighting residues (orange) conserved between FnBRs. Peptide sequences are indicated by a solid bar, and the first and last residue in each peptide that undergoes a >2-Å^2 change in accessible surface area on complex formation are underlined. (*C*) Ribbon diagram for the structures of ^{2}F1^{3}F1/STATT1 and ^{4}F1^{5}F1/STAFF1. Fn modules are shown in cyan, and the FnBR is shown in gray. Strand naming for F1 modules is shown on ^{2}F1. (*D*) Ribbon diagrams for the structures of ^{2}F1^{3}F1/STATT5 and ^{4}F1^{5}F1/STAFF5. The ^{2}F1^{3}F1/STATT1, ^{4}F1^{5}F1/STAFF1, ^{2}F1^{3}F1/STATT5, and ^{4}F1^{5}F1/STAFF5 structures were solved to resolutions of 2, 1.8, 1.7, and 2 Å, respectively. The dotted lines indicate that the orientation between ^{3}F1 and ^{4}F1 was approximated based on the other F1 module interfaces and the short length on the inter-module linker.

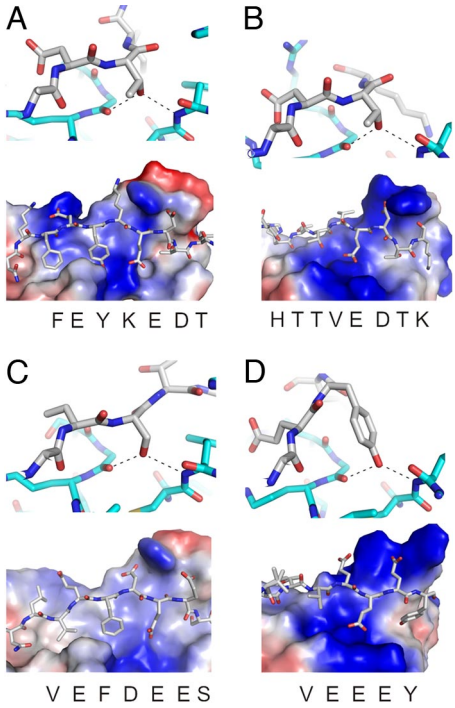

Fig. 2. Specificity of ^{2}F1-peptide and ^{4}F1-peptide interactions. The conserved hydroxyl-containing side-chain threonines ^{4}F1:STAFF1 (*A*) and ^{2}F1:STATT5 (*B*), serine ^{4}F1:STAFF5 (*C*), and tyrosine ^{2}F1:STATT1 (*D*) of the FnBR (gray) forms hydrogen bonds with backbone atoms of homologous residues in ^{2}F1 and ^{4}F1 (cyan). The positions of conserved acidic and hydrophobic FnBR residues (gray) with respect to the electrostatic surface of ^{2}F1 or ^{4}F1 are shown below with FnBR sequences.

interactions with F1 modules, especially at the N- and C-terminal boundaries of the structures in Fig. 1; attempts to crystallize larger complexes have, so far, been unsuccessful.

Comparison of Structures for Identification of the Roles Played by Residues Conserved Between Staphylococcal and Streptococcal FnBRs. The four structures in Fig. 1 reveal the role played by residues conserved between FnBRs (Fig. 1*B*) in binding to the F1 modules. In the ^{2}F1-binding region of FnBRs, an E-D/E-T/S/Y (Fig. 1*B*) motif stands out as being highly conserved, as does a D/E-T/S motif in the ^{4}F1-binding region of the FnBRs (4). Fig. 2 shows that the OH moiety of the hydroxyl-containing side chain, whether a threonine (STAFF1 and STATT5; Fig. 2 *A* and *B*), or a serine (STAFF5; Fig. 2*C*), forms a hydrogen bond with the backbone NH and O atoms of homologous F1 module residues in the D–E loop and A strand. In ^{2}F1, these residues are G100 and F67, respectively, whereas in ^{4}F1, they are G190 and F156. The tyrosine in STATT1 can form the same hydrogen bonds (Fig. 2*D*), but in some structures the side chain is not well ordered, and in another, its orientation is affected by crystal contacts. To accommodate the more bulky tyrosine side chain and maintain the position of the hydroxyl group, there is a change in the peptide backbone orientation. The D/E residue in the ^{2}F1- and ^{4}F1-binding motifs is in close proximity to arginine residues in the E strands of both ^{2}F1 and ^{4}F1 as a result of the register of peptide binding with the E strand. Thus, the D/E-T/S/Y motif appears to play similar roles in ^{2}F1 and ^{4}F1 binding.

The structure of ^{2}F1 in the absence of peptide (PDB ID code: 2CG7) (16), shows that an arginine residue in strand C of ^{2}F1 forms a rather side-on interaction (17) involving Nε with an aspartate residue in strand A, and the terminal NH_2 groups of the arginine are partially solvent exposed. On binding of STATT1 and STATT5, however, these terminal groups are completely buried. In these complexes, a glutamate residue that is fully conserved in the ^{2}F1-binding motifs of all *S. pyogenes* and *S. aureus* FnBRs (4) (**E**-E/D-T/S/Y; Fig. 1*B*) forms an end-on interaction [as has been observed to be favored in intermolecular interactions (17)] with the arginine in strand C (Fig. 2 *B* and *D*). The intramolecular side-on interaction with the aspartate in strand A is also maintained in these complexes. Thus, upon bacterial peptide binding, the conserved glutamate in the ^{2}F1-binding motif would appear to be playing a role in stabilization of what otherwise would become buried charge. In ^{4}F1, the basic residue in strand C is a lysine whose hydrogen-bonding capacity in the presence and absence of peptide appears to be satisfied through the intramolecular interaction with the acidic residue in strand A. The glutamate discussed above is not conserved in the ^{4}F1-binding motifs of FnBRs (4) (Fig. 1*B*) and when a glutamate is present, for example in STAFF1 and STAFF5 (Figs. 1*B* and 2 *A* and *C*), it does not form an intermolecular salt bridge upon binding.

In the ^{4}F1-binding motifs, there is also a conserved hyd-D/E-hyd motif (where hyd is an amino acid with a hydrophobic side chain) that is not present in the ^{2}F1-binding region. This reflects

BIOPHYSICS

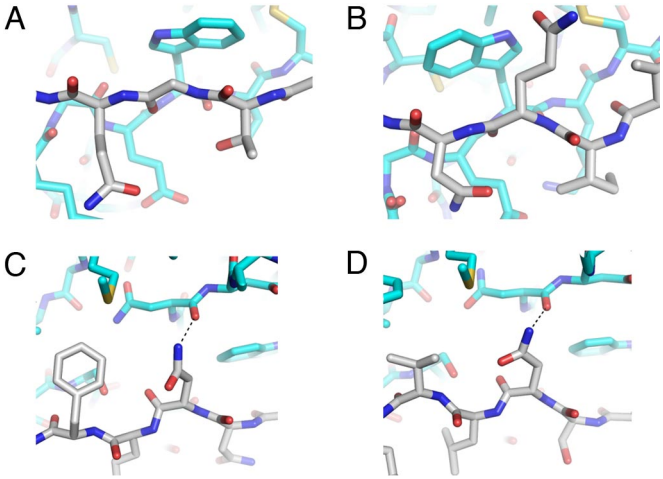

Fig. 3. Role of conserved residues in ^{3}F1 binding and ^{5}F1 binding. (*A*) Structure of ^{2}F1^{3}F1/STATT1 focusing on a conserved glycine residue in the ^{3}F1-binding motif (gray) and a tryptophan in the E strand of ^{3}F1 (cyan). (*B*) Homologous region of ^{4}F1^{5}F1/STAFF1 showing that the different orientation of the tryptophan side chain accommodates a glutamine residue in the bound FnBR. (*C* and *D*) Structures of ^{4}F1^{5}F1/STAFF1 (*C*) and ^{4}F1^{5}F1/STAFF5 (*D*) highlighting the hydrogen bond formed by the conserved asparagine residue of the FnBR (gray) with the backbone of ^{5}F1 (cyan).

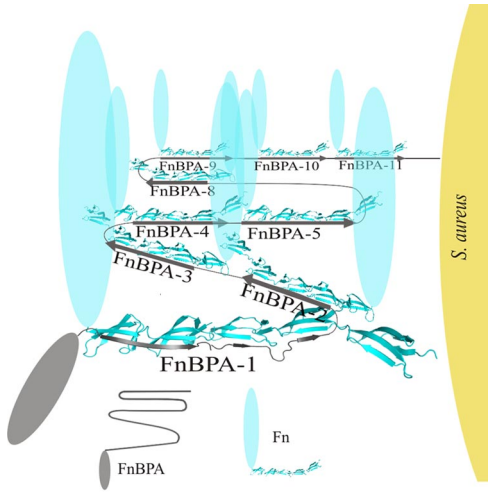

Fig. 4. Efficiency of *S. aureus* binding to Fn. Schematic (not to scale) showing how nine copies of Fn (cyan) might cluster on FnBPA (gray) and illustrating the efficiency of the binding. The five F1 modules from the N-terminal domain are shown with $^{2-5}$F1 (FnBPA-1,5,9,10,11) or $^{3-5}$F1(FnBPA-2,3,4,8) bound to FnBRs through tandem β-zippers, and the remainder of each Fn molecule and FnBPA are shown as cyan and gray ovals, respectively.

several differences between ^{2}F1 and ^{4}F1 at the module surface where this bacterial motif binds. Two hydrophobic pockets are formed on the surface of ^{4}F1 (Fig. 2 *A* and *C*) by several amino acid changes and reorientation of the loop between strands D and E. The conserved acidic residue is adjacent to an arginine residue on the linker between ^{4}F1 and ^{5}F1; the ^{2}F1–^{3}F1 linker has an alanine at this position [supporting information (SI) Fig. S1].

Importantly (because these regions of the FnBRs are less conserved), the structures also shed some light on the interactions of the FnBRs with ^{3}F1 and ^{5}F1 (Fig. 1*B*). A glycine is the most highly conserved residue in the ^{3}F1-binding motifs (4) (Fig. 1*B*) and the reason seems clear. The side-chain orientation of a tryptophan residue in the E strand of ^{3}F1, in both the absence [PDB ID code 2CG7 (16)] and presence of bacterial peptide, is such that only a small side chain allows formation of a regular strand at this point (Fig. 3*A*). The tryptophan is conserved in ^{5}F1 but here, a difference in the side-chain rotamer (χ1 angle) provides room for a glutamine residue in the FnBR (Fig. 3*B*). In STAFF1 and STAFF5, the side-chain NH_2 of the conserved asparagine in the ^{5}F1-binding region (Fig. 1*B*) forms a hydrogen bond with the backbone carbonyl oxygen of an asparagine residue in strand A of ^{5}F1 (Fig. 3 *C* and *D*).

Of further note is the short "looped-out" region observed in the bacterial peptide between ^{2}F1 and ^{3}F1 in the STATT1 (Fig. 1*C*) and STATT5 (Fig. 1*D*) complexes with ^{2}F1^{3}F1. This loop is slightly longer in the STATT1 complex, consistent with the presence of additional residues in this ^{2}F1^{3}F1-binding motif compared with other FnBRs (Fig. 1*B*) (4).

FnBPA-5 has <25% identity (8 of 34 residues) with FnBPA-1 (Fig. 1) (4), yet the tandem β-zipper mechanism of binding is conserved. The position of the asparagine (STAFF1) and glycine (STAFF5) residues (underlined in Fig. 1*B*), that are the most N-terminal FnBR residues participating in the intermolecular interface with NTD, fit well with the length of FnBRs (FnBPA-9,10,11) that bind NTD with high affinity (5) and are predicted to bind four F1 modules (4) (Fig. 1*B*). For FnBRs (FnBPA-2,3,4,8) the N-terminal boundary matches that of the ^{4}F1-binding residues in STAFF1 and STAFF5, consistent with the lack of a complete ^{5}F1-binding motif. Similarly, the position of the most C-terminal interacting residue in STATT1 (tyrosine) and STATT5 (threonine) fits well with the N-terminal boundary of the other FnBRs.

From the early characterization of Fn-binding proteins of *S. aureus* (3) to more recent studies (18), there is good evidence that the interaction with Fn is multivalent, i.e., between six and nine Fn molecules bind a single copy of FnBPA or FnBPB. We (19) and others (20) have suggested that multivalent binding of Fn to bacterial Fn-binding proteins is likely to play a role in invasion of human cells, and this hypothesis is supported by the observation that bacterial Fn-binding proteins from *S. pyogenes* also contain multiple Fn-binding sites (4, 15). Multivalent binding is rather puzzling however, given the relative sizes of NTD (29-kDa) and FnBPA (40-kDa Fn-binding region). The structures in Fig. 1 *C* and *D* show that the interaction of the FnBRs with the F1 modules is almost continuous, and there are very few linker residues between FnBRs. In the absence of Fn, FnBPA constructs containing multiple FnBRs have been shown to be intrinsically disordered by both NMR spectroscopy (21) and circular dichroism (22) studies. The intrinsic disorder before binding, unidirectional strand formation upon binding, and neat matching of FnBR length to bind three or four F1 modules (with few additional linker residues) together would allow the highly efficient clustering of several NTD molecules in a comparatively short section (363 residues) of bacterial protein (Fig. 4).

Many eukaryotic and prokaryotic proteins are predicted to contain substantial regions with no stable secondary structure elements (23). These intrinsically disordered regions (IDRs) can form a significant proportion of the intact protein sequence and are often involved in molecular recognition processes (24). A number of studies have addressed the question of how the protein–protein interactions of IDRs differ from those of folded proteins (12, 25, 26). One clear distinguishing characteristic is the efficiency with which large interfaces are formed with relatively few residues; the FnBPA-1/NTD interaction is an excellent example of this economy. With only 37 bacterial residues, the FnBPA-1/NTD and FnBPA-5/NTD tandem β-zipper interactions each bury $\approx$4,300 Å^2 of accessible surface area. These large interfaces are likely to compensate for unfavorable entropy changes upon complex formation, but may also be required to disrupt Fn–Fn interactions between the NTD and F3 modules (27). The efficiency of the interaction arises because the intrinsic

disorder of the bacterial FnBRs before binding allows a larger percentage of residues to be directly involved in binding (rather than maintaining a stable three-dimensional fold). As has previously been highlighted (25), this is illustrated by the much larger percentage of accessible surface area of the disordered protein (FnBPA-1; 44%) compared with the folded protein ($^{2-5}$F1; 17%) that is buried in the intermolecular interface. When the multivalency (18) is taken into account (Fig. 4), the potential buried surface area in the FnBPA/Fn complex is ≈26,000 Å^2 if only six Fn molecules are bound and ≈36,000 Å^2 if nine molecules are bound. Thus, the 363-residue FnBR region of FnBPA provides an unusual illustration of the efficient formation of protein–protein intermolecular interfaces. We propose that the obvious efficiency of these interactions makes it likely that other IDRs will form similar interactions with Fn or with other multidomain proteins. *S. pyogenes* (15) and the spirochete *Borrelia burgdorferi* (28) appear to use a tandem β-zipper to bind Fn (19). A tandem β-zipper interaction in a different cellular context has also been reported (14).

Intrinsic disorder has been suggested to allow a single protein to bind a number of different proteins acting as "hub" proteins in interaction networks (24). In Fn-binding by *S. aureus*, the intrinsic disorder has been exploited in two different ways. First, it allows the formation of high-affinity interactions of short peptides with a modular protein. Second, when combined with the tandem β-zipper formation, it facilitates the closely spaced binding of multiple copies of Fn. The resultant clustering of integrin-binding sites is likely to play a role in invasion of host cells by *S. aureus*. It has been suggested that interactions between FnBR-bound NTD molecules increase the affinity of FnBR/NTD interactions (18). The mechanism of binding and the closely spaced binding sites that we identified will greatly assist investigations of this possibility in the future.

Animal models of infective endocarditis suggest the importance of *S. aureus*/Fn interactions in disease progression (6), and here, we have shown that they are achieved through a highly unusual mechanism of protein–protein recognition. The large FnBR/$^{2-5}$F1 interfaces suggest that the design of small-molecule inhibitors of the *S. aureus*/Fn interaction will be challenging. However, the design of such compounds and further efforts to understand the role of this interaction in invasion of human cells and in disease will be assisted by the illustration, provided here, of the roles played by residues that are highly conserved across FnBRs of *S. aureus* and *S. pyogenes*.

Methods

Synthetic Peptides and Expression and Purification of Fibronectin Domains. FnBR peptides (Fig. 1*B*) were obtained from Alta Bioscience (University of Birmingham). The ^{2}F1^{3}F1 and ^{4}F1^{5}F1 were expressed in *Pichia pastoris* and purified as described (4).

Crystallization. Crystals were grown by sitting-drop vapor diffusion. Crystals were obtained for ^{4}F1^{5}F1:STAFF1 (0.8 mM/9 mM) in 0.1M Tris·HCl (pH 8.5), 0.15M KSCN, 20% (vol/vol) PEG 400, for ^{2}F1^{3}F1:STATT1 (1 mM/17 mM) in 0.8 M succinic acid (pH 7.0), for ^{4}F1^{5}F1:STAFF5 (1.4 mM/7.4 mM) in 0.2 M NaCl, 0.1 M Bis-Tris (pH 6.3), 14% (wt/vol) PEG3350, and for ^{2}F1^{3}F1:STATT5 (0.8 mM/18 mM) in 0.95 M succinic acid (pH 7.0). Crystals were flash-cooled in liquid nitrogen by using cryoprotectants 30% (wt/vol) PEG 400, 12%, 20%, and 23% (wt/vol) glycerol, respectively.

Data Collection and Refinement. X-ray diffraction data for ^{4}F1^{5}F1/STAFF1, ^{2}F1^{3}F1/STATT1, ^{4}F1^{5}F1/STAFF5, and ^{2}F1^{3}F1/STATT5 were collected at 100 K at the European Synchrotron Radiation Facility on beamlines 14-1, ID29, 14-2, and 14-4. Diffraction data were processed and scaled with HKL2000 (HKL Research Inc.) and MOSFLM/SCALA (29). Structure solution of the ^{2}F1^{3}F1–STATT1 complex was by molecular replacement in PHASER (30). A low-resolution ^{2}F1^{3}F1/STATT1 complex structure was solved by using 2CG7 (16) by molecular replacement, and the coordinates of ^{2}F1^{3}F1 from this model were, in turn, used to solve the structure presented here.

Structure solution of ^{4}F1^{5}F1-STAFF1, ^{4}F1^{5}F1-STAFF5, and ^{2}F1^{3}F1-STATT5 was by molecular replacement in PHASER (30) and MOLREP (31) using several search strategies. Searches were conducted by using whole ^{4}F1^{5}F1 (PDB ID code 1FBR) or ^{2}F1^{3}F1 module pairs and also individual F1 modules. Correct solutions were obtained by manually extracting correctly positioned F1 modules after searching for multiple copies of ^{2}F1 in MOLREP (31).

Structure refinement proceeded by alternating between manual building in COOT (32) and automatic refinement in REFMAC (31). The bacterial peptides were initially built as polyalanine into Fo-Fc density in COOT (32). As refinement proceeded and map quality improved, this allowed unambiguous assignment of sequence to the polyalanine backbone (Fig. S1). A summary of the diffraction data and refinement statistics is available as online Table S1. Figures containing structures (including electrostatic surfaces) were prepared in Pymol (33). Buried accessible surface area was calculated by subtracting areas of the separate components from that of the complex by using Areaimol (34).

ACKNOWLEDGMENTS. This work was supported by a British Heart Foundation Senior Basic Science Research Fellowship (to J.R.P.) and by the Wellcome Trust and the Biotechnology and Biological Sciences Research Council. E.R.-P. thanks the academic exchange program between the Royal Society (London) and the Academia Mexicana de Ciencias and Programa de Apoyo a Proyectos de Investigación e Innovación Tecnológica IN228106-3 for financial support.

1. Lowy FD (1998) *Staphylococcus aureus* infections. *N Engl J Med* 339:520–532.
2. Casey AL, Lambert PA, Elliott TSJ (2007) Staphylococci. *Int J Antimicrob Ag* 29:S23–S32.
3. Froman G, Switalski LM, Speziale P, Höök M (1987) Isolation and characterization of a fibronectin receptor from *Staphylococcus-aureus*. *J Biol Chem* 262:6564–6571.
4. Schwarz-Linek U, *et al.* (2003) Pathogenic bacteria attach to human fibronectin through a tandem beta-zipper. *Nature* 423:177–181.
5. Meenan NAG, *et al.* (2007) The tandem β-zipper model defines high affinity fibronectin-binding repeats within *Staphylococcus aureus* FnBPA. *J Biol Chem* 282:25893–25902.
6. Que Y-A, *et al.* (2005) Fibrinogen and fibronectin binding cooperate for valve infection and invasion in *Staphylococcus aureus* experimental endocarditis. *J Exp Med* 201:1627–1635.
7. Peacock SJ, Foster TJ, Cameron BJ, Berendt AR (1999) Bacterial fibronectin-binding proteins and endothelial cell surface fibronectin mediate adherence of *Staphylococcus aureus* to resting human endothelial cells. *Microbiology* 145:3477–3486.
8. Heying R, van de Gevel J, Que Y-A, Moreillon P, Beekhuizen H (2007) Fibronectin-binding proteins and clumping factor A in *Staphylococcus aureus* experimental endocarditis: FnBPA is sufficient to activate human endothelial cells. *Thromb Haemost* 97:617–626.
9. Fitzgerald JR, Foster TJ, Cox D (2006) The interaction of bacterial pathogens with platelets. *Nat Rev Micro* 4:445–457.
10. Arrecubieta C, *et al.* (2006) The role of *Staphylococcus aureus* adhesins in the pathogenesis of ventricular assist device-related infections. *J Infect Dis* 193:1109–1119.
11. Conte LL, Chothia C, Janin J (1999) The atomic structure of protein–protein recognition sites. *J Mol Biol* 285:2177–2198.
12. Meszaros B, Tompa P, Simon I, Dosztanyi Z (2007) Molecular principles of the interactions of disordered proteins. *J Mol Biol* 372:549–561.
13. Remaut H, Waksman G (2006) Protein–protein interaction through β-strand addition. *Trends Biochem Sci* 31:436.
14. Deane JE, *et al.* (2004) Tandem LIM domains provide synergistic binding in the LMO4:Ldb1 complex. *EMBO J* 23:3589–3598.
15. Schwarz-Linek U, *et al.* (2004) High affinity streptococcal binding to human fibronectin requires specific recognition of sequential F1 modules. *J Biol Chem* 279:39017–39025.
16. Rudino-Pinera E, *et al.* (2007) The solution and crystal structures of a module pair from the *Staphylococcus aureus*-binding site of human fibronectin—A tale with a twist. *J Mol Biol* 368:833–844.
17. Mitchell JBO, Thornton JM, Singh J, Price SL (1992) Towards an understanding of the arginine–aspartate interaction. *J Mol Biol* 226:251–262.
18. Ingham KC, Brew S, Vaz D, Sauder DN, McGavin MJ (2004) Interaction of *Staphylococcus aureus* fibronectin-binding protein with fibronectin: affinity, stoichiometry, and modular requirements. *J Biol Chem* 279:42945–42953.
19. Schwarz-Linek U, Höök M, Potts JR (2006) Fibronectin-binding proteins of Gram-positive cocci. *Microbes Infect* 8:2291–2298.
20. Ozeri V, *et al.* (2001) *De novo* formation of focal complex-like structures in host cells by invading streptococci. *Mol Microbiol* 41:561–573.
21. Penkett CJ, *et al.* (1998) Structural and dynamical characterization of a biologically active unfolded fibronectin-binding protein from *Staphylococcus aureus*. *Biochemistry* 37:17054–17067.
22. HousePompeo K, Xu Y, Joh D, Speziale P, Höök M (1996) Conformational changes in the fibronectin binding MSCRAMMs are induced by ligand binding. *J Biol Chem* 271:1379–1384.
23. Dunker AK, *et al.* (2001) Intrinsically disordered protein. *J Mol Graphics Model* 19:26–59.
24. Uversky VN, Oldfield CJ, Dunker AK (2005) Showing your ID: Intrinsic disorder as an ID for recognition, regulation and cell signaling. *J Mol Recognit* 18:343–384.
25. Gunasekaran K, *et al* (2003) Extended disordered proteins: targeting function with less scaffold. *Trends Biochem Sci* 28:81–85.

26. Sickmeier M, *et al.* (2007) DisProt: the database of disordered proteins. *Nucleic Acids Res* 35:D786–D793.
27. Vakonakis I, Staunton D, Campbell ID (2007) Interdomain association in fibronectin: insight into cryptic sites and fibrillogenesis. *EMBO J* 26:2575–2583.
28. Raibaud S, *et al.* (2005) *Borrelia burgdorferi* binds fibronectin through a tandem beta zipper- a common mechanism of fibronectin binding in staphylococci, streptococci and spirochetes. *J Biol Chem* 280:18803–18809.
29. Leslie A (2006) The integration of macromolecular diffraction data. *Acta Crystallogr D* 62:48–57.
30. McCoy AJ, *et al.* (2007) Phaser crystallographic software. *J Appl Crystallogr* 40:658–674.
31. Collarorative Computational Project Number 4 (1994) The CCP4 suite: programs for protein crystallography. *Acta Crystallogr D* 50:760–763.
32. Emsley, P. Cowtan K (2004) Coot: Model-building tools for molecular graphics. *Acta Crystallogr D* 60:2126–2132.
33. Delano WL (2002) *The PyMOL Molecular Graphics System*. (DeLano Scientific, Palo Alto, CA).
34. Potterton E, Briggs P, Turkenburg M, Dodson E (2003) A graphical user interface to the CCP4 program suite. *Acta Crystallogr D* 59:1131–1137.